Nuclear Instruments and Methods in Physics Research A274 (1989) 113–128
North-Holland, Amsterdam

CALIBRATION OF THE L3 BGO ELECTROMAGNETIC CALORIMETER WITH A RADIOFREQUENCY QUADRUPOLE ACCELERATOR

H. MA, R. MOUNT, H. NEWMAN, F. ROEBER and R. ZHU *
California Institute of Technology, Pasadena, CA 91125, USA

H. AKBARI, C.Y. CHIEN and A. PEVSNER **
John Hopkins University, Baltimore, MD 21218, USA

R. HAMM
AccSys Technology, Inc., Pleasanton, CA 94566, USA

Received 30 June 1988

A new calibration technique based on radiative capture of protons from an RFQ accelerator in a lithium target, which makes use of the resultant high intensity flux of 17.6 MeV photons, has been developed and tested. The technique is capable of calibrating the thousands of BGO crystals in the L3 electromagnetic calorimeter at once, with an absolute accuracy of better than 1% in 1–2 h. Systematic errors in the calibration, which have been studied earlier through Monte Carlo simulations, have been experimentally proven to be small and calculable, and are expected to be much less than 1%. When installed in the L3 experiment at LEP, this system will help ensure that the high resolution of the L3 electromagnetic calorimeter is maintained during running.

1. Introduction

The L3 electromagnetic calorimeter, which is composed of 11 000 large bismuth germanate ($Bi_4Ge_3O_{12}$) crystals, has been designed to provide precise energy measurements of electrons and photons, from less than 100 MeV up to 100 GeV [1]. L3's ability to detect new physics processes, such as $e^+e^- \rightarrow Z^{0*}$ + Higgs → e^+e^- + Higgs, depends on the resolution of the BGO array, and hence on the quality of the calibration. Achieving this resolution will hinge on accurate and frequent gain calibrations in situ.

The need for rapid, precise calibrations has been established by CMU, CERN and Caltech groups in L3 [2–4]. Sustained radiation doses of 1 rad/h or more, or a shot of a few rads in standard production quality BGO crystals [5], will cause apparent gain shifts of 1% or more. This radiation rate may be expected during injection at LEP, during stable beam periods when the orbit of the LEP beam is not perfect, or whenever the vacuum upstream of the experiment is poor.

After four years' study of potential calibration techniques, we have found that a 1.6 MeV Radiofrequency Quadrupole (RFQ) proton accelerator may be used to bombard a lithium target. This produces a high intensity flux of 17.6 MeV photons by radiative capture ($^7_3$Li(p, γ)$^8_4$Be), which acts as a calibration source. The photon flux produced is sufficient for calibrations more than once per day, or on a continuous basis by pulsing the RFQ at a low duty cycle during physics runs at LEP. The complete procedure between LEP data-taking runs will take approximately 1 h, for a high statistics precise calibration.

The *RFQ Project* has been conceived and developed by the Caltech group. Early tests at Van de Graaff at Lyon University as well as Caltech and a substantial series of Monte Carlo studies [6] helped to establish the feasibility of this technique. The first of a series of tests with an actual RFQ took place in March, 1986, at Los Alamos. A major step was taken in November of 1987, with a successful realistic test of a BGO crystal array with photodiode readout at an RFQ at AccSys Technology, Inc. [7]. A precision better than 1% has been achieved in this test.

This report describes the RFQ-based BGO calibration and summarizes the results of the test at AccSys. Section 2 describes the L3 RFQ system design. A brief summary of the Monte Carlo simulation results is given in section 3. Section 4 outlines the setup and the running conditions at AccSys. The data analysis and results of the test are presented in section 5.

* Supported in part by U.S. Department of Energy Contract No. DE-AC03-81-ER40050.
** Supported in part by NSF Contract No. PHY-19556.

2. The L3 RFQ system

The RFQ is a quasielectrostatic accelerator, with advantages of a high beam current and very compact size (up to 100 mA of protons). An RFQ has been the accelerator of choice (especially over the last four years) whenever acceleration of intense H^+, H^- or heavy ion beams up to a fixed energy in the range from 750 keV to 2.5 MeV is required [8]. RFQs are in use for a variety of applications at CERN, Saclay, BNL, DESY, Los Alamos and elsewhere; they are the preinjectors for all CERN proton beams now, and for HERA in the future. Other low energy accelerators, such as Van de Graaffs, are inadequate for our purpose because of our requirements for high peak current and small machine size.

The major components of the RFQ system for L3 are:

(1) an H^- ion source, and low energy beam transport (LEBT);
(2) a 1.6 MeV RFQ accelerator;
(3) high energy beam transport (HEBT);
(4) beam neutralizer ($H^- \rightarrow H^0$) consisting of a differentially pumped water vapor or noble gas cell;
(5) rf power system;
(6) vacuum system;
(7) control and monitoring systems;
(8) lithium target;
(9) calibration data acquisition and readout systems.

Fig. 1 is a block diagram of the AccSys RFQ system. The principal specifications of the RFQ acceleration system are summarized in table 1. Simulated beam trajectories are shown in fig. 2. Fig. 3 shows the distributions of the proton energy, phase and positions, after acceleration in the RFQ.

Table 1
AccSys RFQ specification

Accelerated particle species	H^+
Input ion energy	30 keV
Normalized input emittance (95%)	$< 0.04\pi$ cm mrad
Nominal current limit	63 mA
Nominal phase-space acceptance	0.116π cm mrad
Final synchronous phase	30°
Nominal output energy	1.92 MeV
Operating frequency	417.7 MHz
Beam pulse width	1–50 μs
Beam repetition rate	1–150 Hz
Input beam current (pulse)	35 mA
Intervane voltage	65 kV
Maximum surface gradient	35 MV/m
Required rf power (pulsed)	200 kW minimum
Output beam current (pulsed)	30 mA
Residual vacuum	$< 1 \times 10^{-6}$ Torr
Normalized output emittance (90%)	$< 0.06\pi$ cm mrad
Output energy spread (90%)	$< \pm 20$ keV
Output phase spread (90%)	$< \pm 15°$

The plan to install the RFQ in the L3 experiment is shown in fig. 4 (including the BGO end caps which will be installed after LEP startup). The RFQ will be situated below the LEP machine, and the neutralized hydrogen atom beam will go through the detector via a beam pipe at an angle of 21.6° with respect to the LEP beam line. The beam will be focused to a 2 cm diameter spot, matching the active area of the target, 10 m from the RFQ. Because the normalized emittance of the beam will be approximately 0.05π cm mrad, the HEBT and neutralizer can be relatively small, and a narrow vacuum tube will suffice. The RFQ vacuum tube, which is

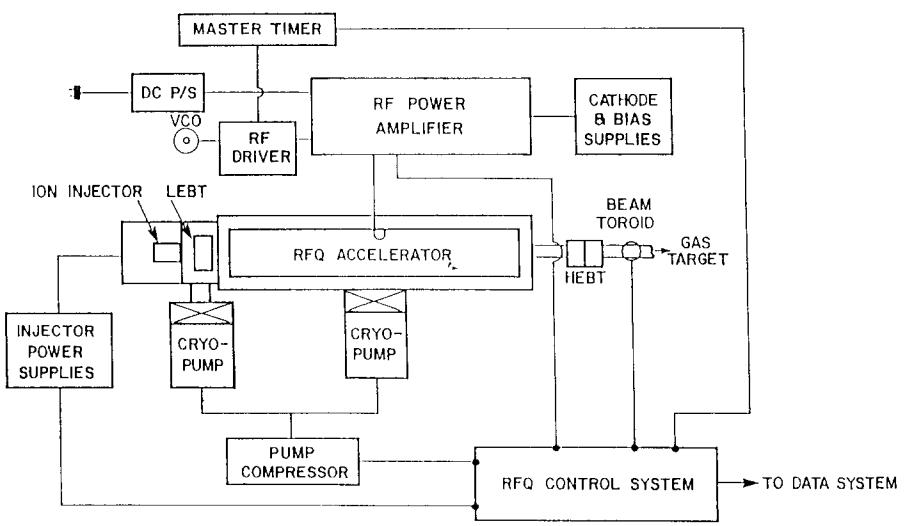

Fig. 1. A block diagram of the AccSys RFQ system.

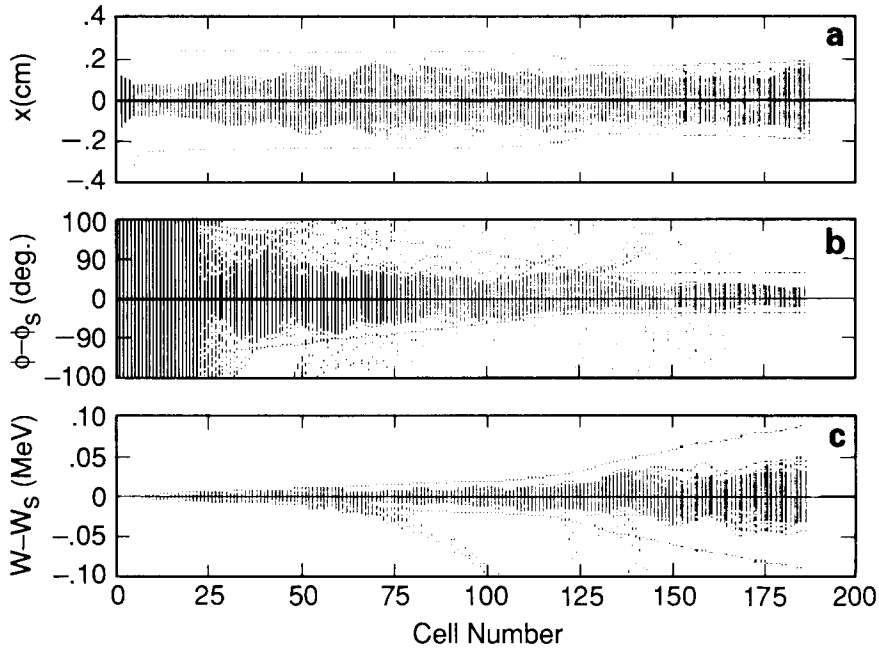

Fig. 2. Simulated beam transport in the AccSys RFQ of H^+ ions; (a) transverse beam size, (b) deviation from the synchronous phase and (c) deviation from the nominal energy, are shown for an ensemble of particle orbits. The cell number (1–186) is plotted on the abscissa.

entirely separate from the 10^{-9} Torr LEP vacuum system, will terminate at a lithium target situated next to the end wall of the time expansion chamber (TEC) vertex detector. The vacuum required in the RFQ tube, to avoid reionization of the neutralized beam, is in the 10^{-6} Torr range.

Because the RFQ target position is off center, the radiative capture photons will enter some crystals at angles up to 60° with respect to the crystal normal. Simulations of the conversion, scattering and absorption of the photons [6] have shown that good energy spectra may be obtained even in the most unfavorable cases, resulting in a precise calibration.

The high RFQ beam intensity is needed to allow us to run the accelerator at a low duty cycle in a pulsed mode. This allows the BGO readout system to trigger on an external strobe derived from the start of the RFQ pulse. This mode is similar to the way the readout will work during data taking at LEP, where it will be strobed and all analog inputs reset just before the arrival of the electron and positron bunches.

The RFQ pulsing scheme must satisfy a number of constraints:

(1) Each RFQ pulse must be short: no more than a few μs to allow for a short integration time for BGO pulses arriving soon after the trigger of the readout system, thus keeping a low readout noise (> 0.9 MeV equivalent) [1].

(2) During an RFQ pulse, the beam intensity must be high enough so that the total rate of photons produced by radiative capture allows for calibration of all 11 000 BGO crystals in 1 h.

(3) The total pulsing rate is limited by the maximum data acquisition rate of the L3 BGO readout system.

These requirements have led to the following beam specifications:

(1) Pulse width: 3 μs.

(2) Beam intensity during the pulse: up to 12 mA on the lithium target, or up to 24 mA before the neutralizer.

(3) Pulsing rate: 150 Hz.

3. Simulation studies of RFQ calibration

A systematic simulation study of the feasibility of the RFQ calibration scheme was carried out by Zhu [6]. The calibration point was chosen to be the "HH^+" energy, defined as the energy at which the upper edge of the spectrum falls to half its maximum height. Using the SLAC EGS program [9], the systematic changes in the HH^+ point were studied, as a function of the following factors:

(1) the position and angle of the normal of a photon incident on a crystal;

(2) the cut on the energy deposited in the adjacent crystals, used in selecting events;

(3) the 0.2 mm carbon fiber walls between the crystals;

(4) the TEC chamber aluminum end wall between the target and the crystals;

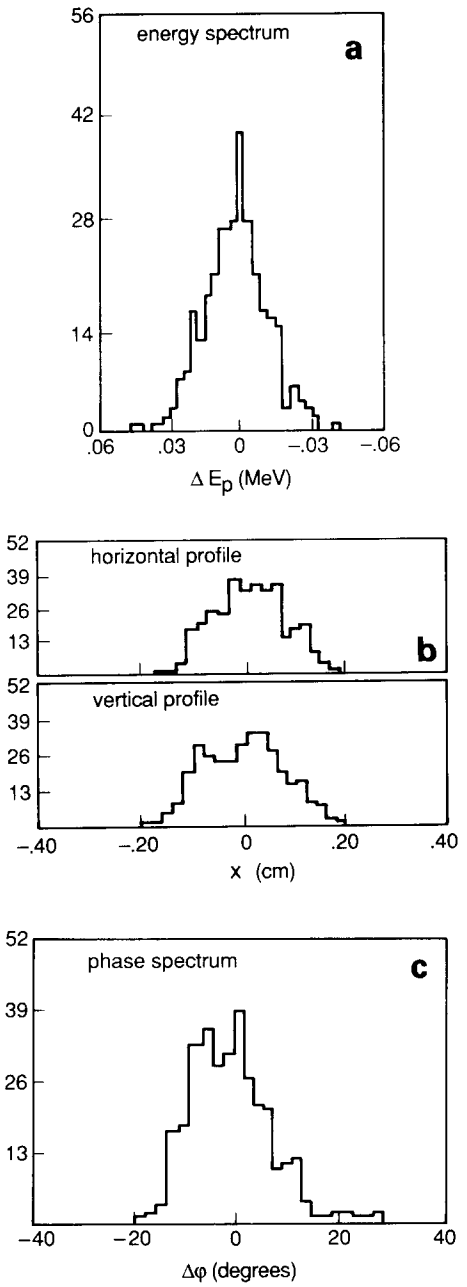

Fig. 3. Proton energy (a), position (b) and phase (c) distributions after being accelerated in RFQ.

(5) the electronic noise in the BGO readout, which may vary with time;
(6) radiation damage in the crystals, which may have varying depth profiles, and which will vary with time.

The details of the simulation can be found in ref. [6]. The variations of the calibration point due to the various factors can be summarized as follows:

(1) Variation of the incident angle from 0° to 25°, and to 50°; the calibration point changes of −0.7% and −1.8%, respectively, relative to the value at 0°.
(2) Variation of the cut used on the neighboring crystals to select events, from "no cut" to a 4 MeV cut and a 2 MeV cut: the calibration point changes +0.3% and +1.8%, respectively. A fixed energy cut determined within the error given by the BGO resolution will result in a systematic effect of $\lesssim 0.1\%$.
(3) Variation of the wall thickness of the carbon fiber structure that holds each crystal (nominal value 0.2 mm) from 0 to 0.5 mm: the calibration point changes less than 0.2%.
(4) Variation of the material in front of BGO, such as the TEC end wall: since 98% of the crystals see an effective thickness of less than 6 cm of aluminum, and all see less than 20 cm, the associated variation in the calibration point is less than 0.6%.
(5) Variation of the noise from 0.6 MeV to 1.6 MeV: less than 1%.

Since the factors in (1) to (4) are fixed in the experiment for each individual crystal, it is trivial to take this small variation into account. The total systematic shift from these factors will be much less than 1%. A measurement of the noise level, by measuring the width of the pedestal in each channel, will further reduce the effect in (5) to much less than 1%. The simulations thus have provided compelling evidence that a 1% calibration based on this technique is feasible.

4. RFQ calibration test at AccSys

A milestone test of the RFQ calibration technique was carried out at AccSys, in November 1987. The aims of the test [10] were:

(i) to prove that the RFQ calibration technique can achieve better than 1% accuracy, under realistic running conditions, and
(ii) to test the EGS computer simulation's predictions for the energy spectrum used in the calibration [6]; to verify that variations of the calibration point arising from the angle of incident of the photons, and the amount of material in front of the crystals, lead to very small and calculable systematic effects.

As summarized in section 5, an accuracy better than 1% was achieved. The small shifts of the calibration point, caused by varying the angle of incidence of the photons and by inserting a relatively thick absorber (5 cm aluminum), agree with the predictions of the Monte Carlo simulations.

4.1. AccSys RFQ beam

The AccSys RFQ provided a proton (H^+) beam that met most of our requirements for the test [10]: (1) beam

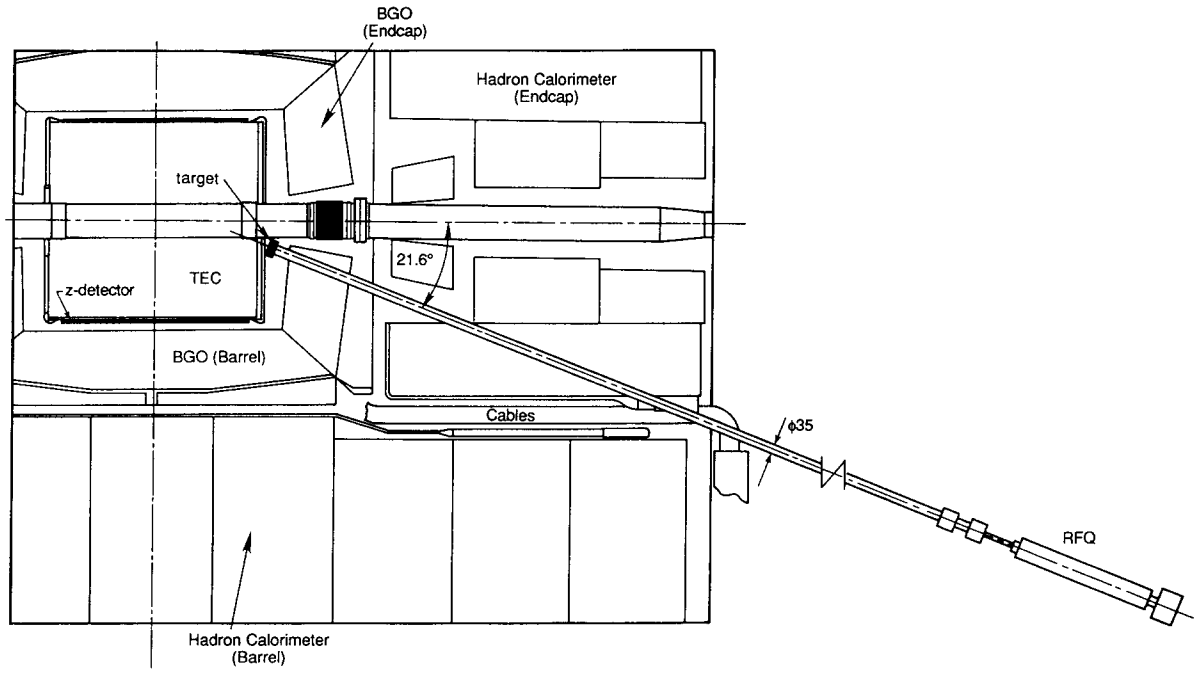

Fig. 4. Plan of RFQ beam tube installation in the L3 detector.

energy: 1.92 MeV: (2) pulse repetition rate; 60 Hz; (3) pulse width: 3 μs; (4) peak current on target: 2–8 mA.

The beam energy was well-matched to our target design, as specified in section 4.2. The maximum pulse rate of AccSys RFQ could be upgraded to 150 Hz, but our readout system (prior to a recent upgrade) could only reach a maximum of 90 Hz at the time of the test. The 3 μs pulse width matched the design value for the

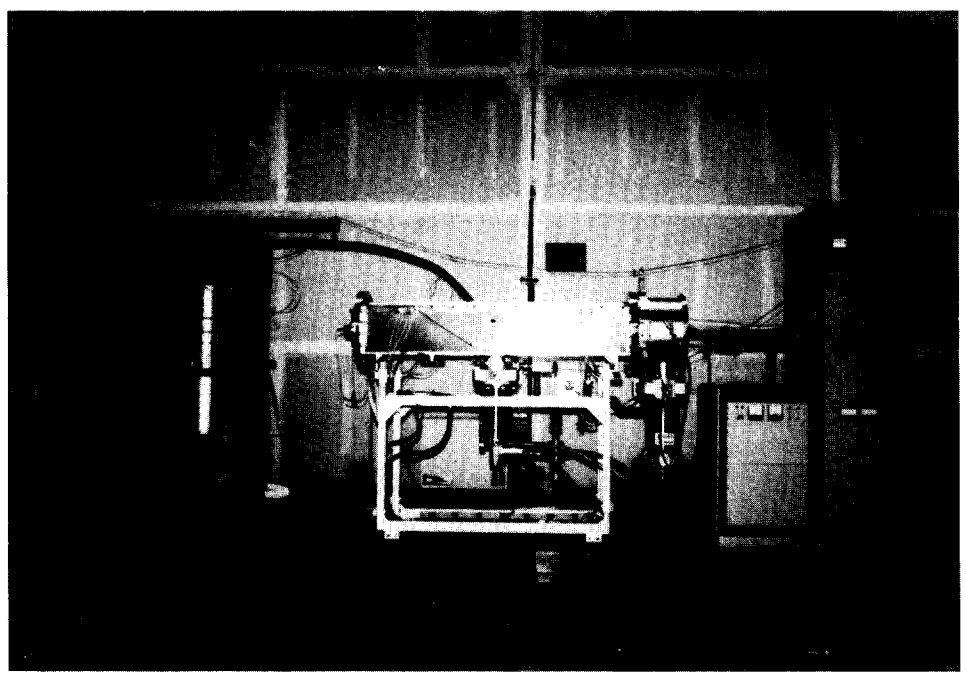

Fig. 5. A photograph of the AccSys RFQ.

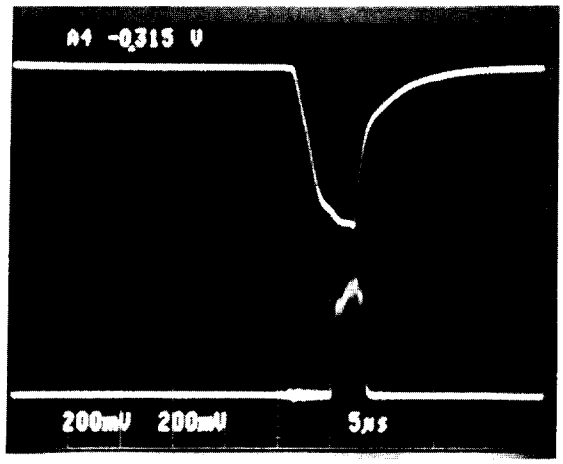

Fig. 6. Rf pulse and beam pulse of the AccSys RFQ.

final RFQ system, and we were able to test narrower pulse widths down to 1 μs as well.

Fig. 5 is a photograph of the RFQ system. Fig. 6 is a picture of beam monitor output signals, taken during the test at AccSys, showing a very clean 3 μs wide 4 mA beam pulse together with the RF pulse.

The AccSys RFQ is capable of supplying up to 30 mA of beam current. For crystals at 50 cm from the target, the nominal beam charge on target is 1.7 nC/pulse [10] (or 0.6 mA × 3 μs), corresponding to 200 photons produced over the full solid angle. For the standard L3 size crystal, which is 2 × 2 cm^2 in the front, 3 × 3 cm^2 at the back and 24 cm in length, this corresponds to 2% hit probability per beam pulse. Taking into account the 40% efficiency predicted by the Monte Carlo studies [6], the rate of photons with energies larger than 14 MeV seen by a crystal is about 0.8% per pulse. A larger beam charge per pulse will cause a higher double hit rate. Since the events with double hits have to be excluded from the analysis by using a veto cut on the energy deposited in neighboring crystals, a high current beam would not speed up the calibration procedure.

We used a simple setup, consisting of a small bending magnet (already available at AccSys), but no beam focusing quadrupoles for the test. One disadvantage of this setup was that the beam was defocused by the bending magnet, and much of the beam did not strike the active area of the target. This caused an uncertainty of the integrated charge on the lithium during running, and prevented us from obtaining a measurement of the exact data acquisition efficiency, relative to the charge on target. The integrated charge per pulse on target was estimated to be in the range of 1–4 nC.

In summary, the beam parameters obtained at AccSys were close to those needed for operation in L3. The main differences were: (1) the beam was not neutralized, and (2) the pulse rate was lower. We will test the 150 Hz repetition rate with our upgraded readout system this year. The neutralized beam will only be available once the L3 RFQ system is built.

4.2. Target

T. Lawrence, an undergraduate then at Caltech, designed a lithium target in 1985, with a 7 μm stainless steel window to encapsulate the lithium metal. This target was proven to be suitable for use in our Van de Graaff test at the Caltech Kellogg Lab in 1985 and our RFQ test at the Los Alamos Accelerator Test Stand in 1986, in which we measured the radiative capture rates and backgrounds. The prototype target, however, would not survive indefinitely at the highest beam intensity for normal running, which is equivalent 8.6 W average. The other shortcoming of the prototype was that the stainless steel foil and the aluminum washer were found (at our Los Alamos RFQ test with a 2 MeV proton beam) to produce substantial radiative capture backgrounds. A series of tests at the Caltech Kellogg Van de Graaff subsequently showed that molybdenum gave much lower backgrounds than steel, copper and aluminum.

The target used in the AccSys test was designed by F. Roeber in which molybdenum is the only material struck by the beam, as shown in fig. 7. This eliminates low energy photon background from radiative capture in aluminum and stainless steel. The 15 μm thick molybdenum foil in the lithium target reduced the beam energy to 520 keV. Protons then slowed down in the lithium hitting the 441 keV resonance, while avoiding another undesired resonance at 1.03 MeV.

This target was tested extensively up to 12 W average beam power during a test at the Kellogg Van de

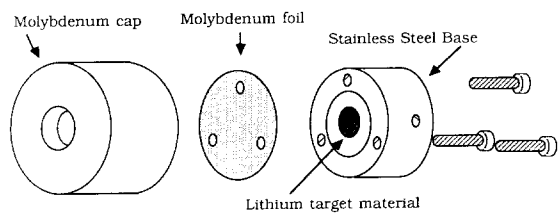

F. Roeber Lithium Target

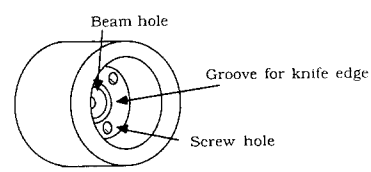

Reverse angle view of molybdenum cap.

Fig. 7. The lithium target design.

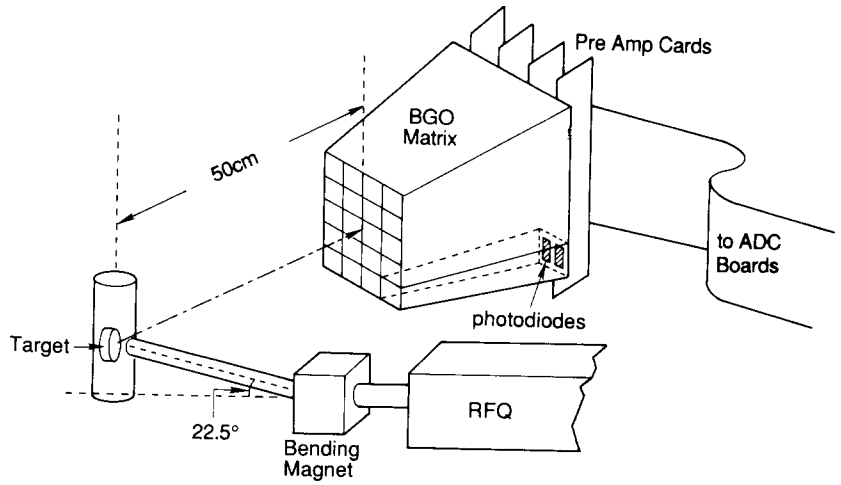

Fig. 8. Schematic drawing of the test matrix setup.

Graaff at Caltech in 1987. The target survived continuous running at AccSys for several days, equivalent to approximately two months' use at LEP, with no apparent aging.

4.3. The test setup

R.Y. Zhu and H. Ma have developed a portable three level BGO readout system for this test. This system is designed to be very close to the final BGO readout system in the L3 detector. The analog electronics which is crucial for the test is identical to the final system. For the sake of simplicity (and cost), the portable system eliminates some of the intermediate VME-based digital readout levels which are used in L3, and which are not needed for a small test setup.

Fig. 8 is a schematic drawing of the test matrix setup. Fig. 9 is a block diagram of the readout system. The test setup consists of the following hardware devices:

(1) 20 L3-size BGO crystals each with two Hammamatsu 1.5 cm^2 silicon photodiodes, and 8 thermistor temperature sensors installed inside the array;
(2) 20 preamplifiers designed and constructed by the Lyon University;
(3) two 10-channel ADC boards with Hitachi HD637B05 microprocessors (Motorola 6805 equivalent, running at 8 MHz), and resettable integration designed and constructed at Princeton, acting as the Level 1 readout;
(4) one homemade EPROM-based interface board between the HD637B05 and 68000 ECB, acting as a synchronized trigger card;
(5) a modified Motorola 68000 ECB board (4 MHz) used as a Level 2 microprocessor;
(6) a homemade CAMAC FIFO module used as a data buffer between the Level 2 68000 ECB and the Level 3 VAXStation II computer;
(7) a VAXStation II computer with graphics terminal and TK50 cartridge tape playing the role of Level 3 and up.

This system requires a synchronized trigger from the RFQ, to start the time sequence of the ADC and to interrupt the HD637B05. The integration time was adjustable from 6 to 16 μs in 1 μs steps by changing the EPROM in the interface. 8 μs integration time was used in our test to accommodate the 3 μs beam pulse width

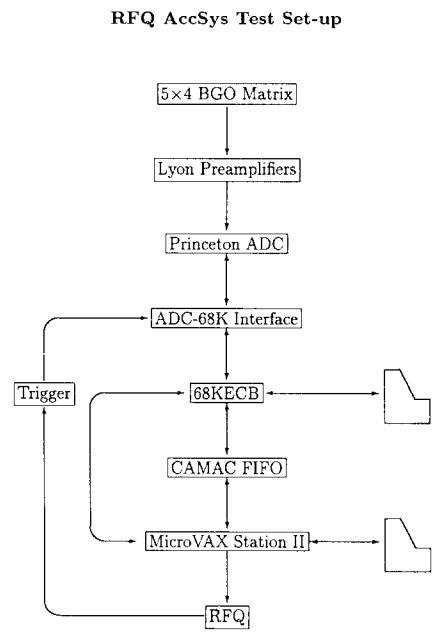

Fig. 9. A block diagram of the readout system.

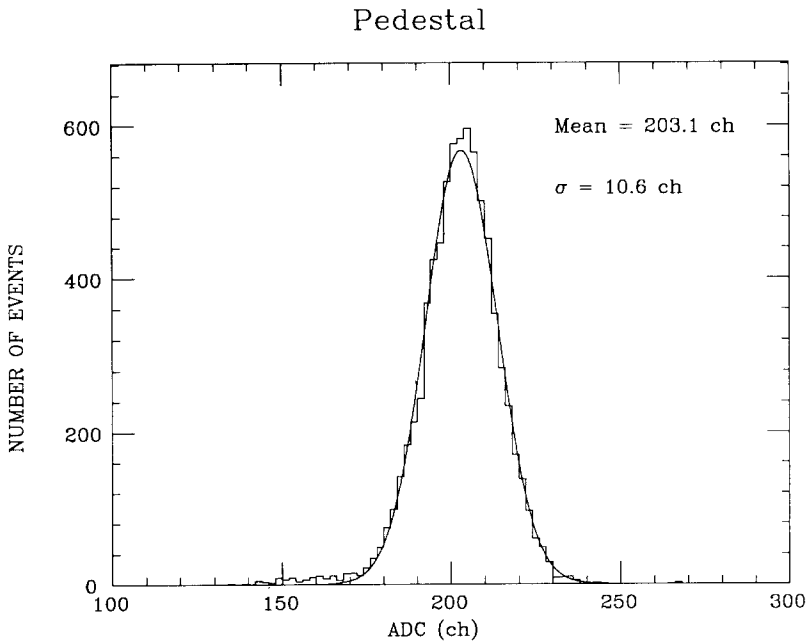

Fig. 10. A typical pedestal distribution together with a Gaussian fit.

plus the 5 μs needed to integrate the signal from the shaping amplifiers.

The software in the 68000 ECB microprocessor controls the Level 1 token passing ring. Data read from Level 1 are checked, packed into an event and sent to a CAMAC FIFO. An interactive data acquisition program running in the VAXStation II receives the data from the CAMAC FIFO via DMA, optionally displays histograms and/or records the data on a hard disk. Data files are backed up on cartridge tapes (TK50) after a few runs.

The readout system was tested extensively prior to the beam test at AccSys. The maximum data acquisition rate was 125 Hz (without histograms) or 90 Hz (with histograms), which is sufficient for the 60 Hz repetition rate provided by the AccSys RFQ. With another random trigger interface board, the system was used in a cosmic ray test at Caltech to determine the rough gains of crystals. The temperature sensors were tested and calibrated at Caltech.

In tests of the electronic noise level at Caltech and AccSys, we observed and average rms noise of 1200 electrons. This is compatible with the figure obtained with the standard L3 BGO readout systems at CERN [11]. Fig. 10 shows a typical pedestal distribution together with a Gaussian fit. The pedestal width of 10.6 channels corresponds to 1200 electrons, or 0.9 MeV equivalent for a typical L3 production-quality crystal. The AccSys test also showed that a well-shielded rf power system will be needed, and that pickup will not be a problem with a properly designed system.

Because the BGO crystals in the test array were obtained from an early series of crystals used at the L3 Cornell tests in 1985, the average light output of the crystals, 900 electrons/MeV, was 1/3 less than the average light output of L3 crystals at CERN. Table 2

Table 2
Test matrix crystal quality

ID	HH^+	kilo-electrons	channels/MeV	ke/MeV
1	148.09	17.77	8.51	1.02
2	135.16	16.22	7.77	0.93
3	142.86	17.14	8.21	0.99
4	128.79	15.45	7.40	0.89
5	127.09	15.25	7.30	0.88
6	113.25	13.59	6.51	0.78
7	144.40	17.33	8.30	1.00
8	148.73	17.85	8.55	1.03
9	135.00	16.20	7.76	0.93
10	115.70	13.88	6.65	0.80
11	135.03	16.20	7.76	0.93
12	138.42	16.61	7.95	0.95
13	162.58	19.51	9.34	1.12
14	127.25	15.27	7.31	0.88
15	152.75	18.33	8.78	1.05
16	117.40	14.09	6.75	0.81
17	115.42	13.85	6.63	0.80
18	126.45	15.17	7.27	0.87
19	106.24	12.75	6.11	0.73
20	102.03	12.24	5.86	0.70
Average	131.13	15.74	7.54	0.90

Table 3
Test runs at AccSys

Run no.	Distance [cm]	Inc. angle [deg]	Al [cm]	No. of events k	Target
2	50	0	0	250	Li
3	50	50	0	240	Li
4	50	30	0	204	Li
5	50	0	5	230	Li
7	50	0	0	250	Li
8	~25	0	0	100	Li
9	50	30	0	190	Li
10	50	50	0	280	Li
11	50	50	5	296	Li
12	50	60	0	260	Li
13	50	0	5	300	Li
14	50	0	0	167	Mo only
15	50	0	0	233	B
16	50	0	0	260	Li
17	50	60	0	317	Li
18	75	0	0	22	Li
19	50	0	0	320	Li [a]

[a] The pulse width for this run was reduced to 1 μs.

lists the crystal quality, showing the absolute gain of each crystal in the matrix.

4.4. Running conditions

In order to maintain an accuracy better than 1% during the run, an "internal pedestal" system was devised in which a control signal from the readout system was used to shut down the ion source for 2 s every minute. This gave 120 pedestal counts each minute, which were used to track apparent pedestal shifts caused by the pickup from the imperfectly shielded prototype rf power system [12]. Temperature readings were also recorded every 5 min, and off-line corrections were made to compensate for the relative change in the BGO light output.

Running conditions were chosen to closely approximate the actual L3 BGO calibration environment, as summarized in table 3. Two complete run cycles were carried out, in order to check the calibration stability. In the "standard" runs, the crystal array was placed 50 cm away from the target, with photons normally incident on the front surface. Runs were also taken in which the crystal array was tilted by 30°, 50° and 60° to test the systematic shift of the calibration point and to compare with the Monte Carlo simulations. We also placed 5 cm of aluminum in front of the BGO array to simulate the TEC chamber end-walls in the L3 experiment.

As mentioned in section 4.1, the RFQ beam current was adjusted so that the probability per beam pulse of having one photon (above 14 MeV) seen in one crystal for each pulse was about 0.8% for the standard runs. This allowed us to avoid double hits.

To investigate the systematic error introduced by double hits, a special run (run 8) was carried out in which the detection probability per crystal per pulse was increased to about 2.5%.

5. Data analysis and test results

5.1. HH^+ determination

The data analysis was done off-line by H. Ma. The raw data were first filtered through a pass 1 program which selects events with at least one energetic hit (larger than 6 MeV) in any of the 20 crystals. The pedestal events and the temperature-measurement data blocks were selected during this pass. The "local pedestals" corresponding to each minute's data, and the calculated temperatures, were written to separate files.

In a second pass, the obtained spectrum of each crystal was first corrected to overcome the intrinsically uneven binning because of the poor differential linearity of the successive approximation ADC. The correction factors were derived by shifting the contents of the neighboring bins of typical pedestal data with high statistics to minimize the χ^2 of the Gaussian distributions. The data were then pedestal-subtracted, giving the energy spectrum for each crystal. Although there was no cooling and temperature control system for our setup, it was found that the temperature variation within a run was less than 0.2° C. Temperature corrections were therefore made for the calibration point, HH^+, after the complete first round analysis for an entire run.

A veto option could be selected, so that an event was accepted only if each of the 8 neighboring crystals had a deposited energy less than E_{VETO}. This veto cut was used to reject two kinds of events: events with a photon whose energy was shared by two neighboring crystals, and events with more than one photons hitting two neighboring crystals. This cut was important only in the high-proton-rate test run.

A spline fit was then applied to the upper edge of the obtained spectrum to determine a piecewise continuous cubic function which closely represents the data without bias. The function was defined in n equal intervals in the fit region with continuous derivatives at the boundaries up to the second order. The number of intervals was chosen to be 7 to accommodate about 100 channels in the fit region, while avoiding local spurious peaks in the fit. A χ^2 was defined as the quadratic sum of the ratios of the deviations of the function from the data to the errors of the data. An analytical minimization of the χ^2 uniquely determined parameters of the function (see Appendix A for details). The resultant function represented the data very well. The bias, de-

Table 4
HH^+ determination and its error of run 7 with spline and B-spline fit; the average and deviation of HH^+ points of a set of simulated spectra based on the spline fit are also given; temperature corrections are not applied

Crystal no.	x_{HH^+} (spline fit)	x_{HH^+} (B-spline fit)	x_{HH^+} (simulation)
7	143.59 ± 1.20	143.41 ± 1.29	143.48 ± 1.10
8	148.30 ± 1.24	148.04 ± 1.27	148.16 ± 1.19
9	135.72 ± 1.24	135.34 ± 0.88	135.49 ± 1.10
12	137.65 ± 1.13	137.12 ± 1.07	137.41 ± 0.98
13	160.98 ± 1.24	161.34 ± 1.10	160.96 ± 1.21
14	125.96 ± 1.09	126.44 ± 0.82	125.78 ± 1.04
Average	± 1.19	± 1.07	± 1.10

fined as the algebraic sum of the deviations between the data and the spline fit, was found to be zero to high precision.

The calibration point HH^+ was then determined from the spline function by using a numerical successive approximation method.

5.2. Statistical error of HH^+

The statistical error of the HH^+ point for 2×10^5 triggers, corresponding to 1600 events above 14 MeV in each crystal's energy spectrum, was computed to be approximately 0.8%. The computation of the error was based on: (1) the rms of the distribution of HH^+ points obtained from fits to a series of Monte Carlo-simulated spectra, generated according to the spline fit to the data, and taking into account the statistical fluctuations in each bin; and (2) an analytical calculation, consisting of propagating the error through the fitting procedure. The details of the error computation are described in Appendix A. As shown in table 4, the uncertainties determined by the cubic spline fit and the cubic B-spline fit, as well as by the Monte Carlo simulation, are consistent. The calculations are also consistent with the deviations of the HH^+ points among the repeated runs with identical conditions.

5.3. Energy spectrum comparison with Monte Carlo

Fig. 11 shows a typical photon energy spectrum together with the molybdenum background obtained from run 14, normalized to the same number of triggers. It is clear that the effect of the molybdenum background is negligible.

Spectra obtained from the six central crystals in the array, together with the spline fit are shown in fig. 12 The data shown have no veto cut. The HH^+ values and the efficiency are also shown, where the efficiency is defined as the ratio of the sum of the number of events with deposited energy greater than 14 MeV to the total number of triggers. It is clear from the figure that for good crystals under standard conditions the calibration point can be obtained without using the veto.

A comparison of three spectra, obtained from one of the central crystals (crystal number 8) for three different veto cuts: no veto, 5 MeV veto and 3 MeV veto respectively, is shown in fig. 13. The mild dependence of the HH^+ value on the veto cuts can be explained by the effect of multiple hits, which was not included in the Monte Carlo simulation.

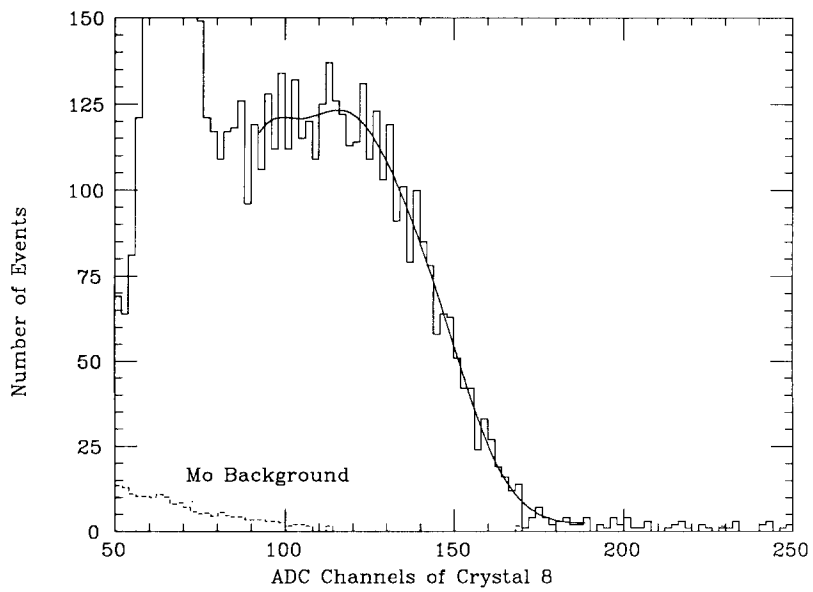

Fig. 11. A typical photon energy spectrum (solid line) and the normalized molybdenum background (dashed line).

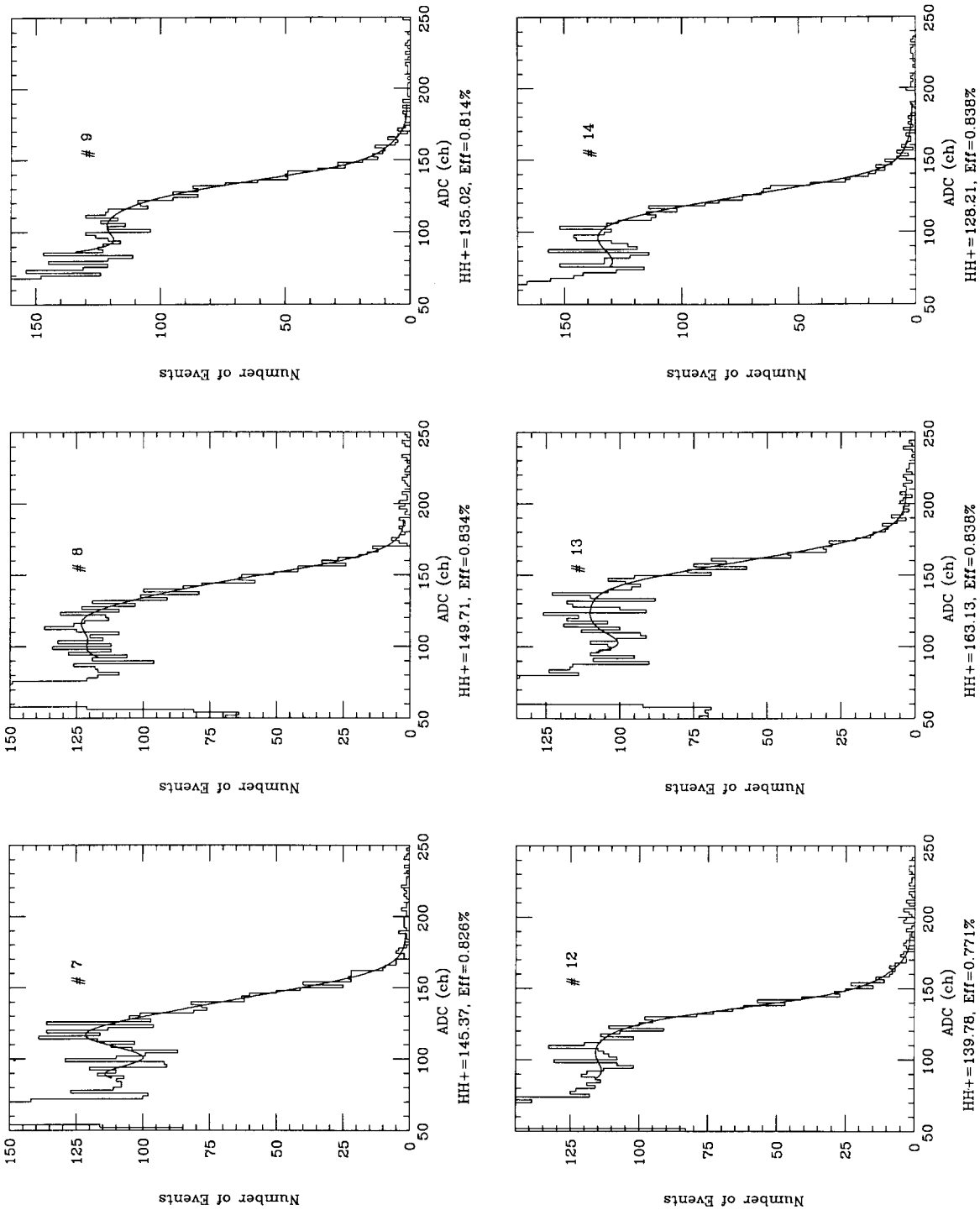

Fig. 12. Photon energy spectra and HH^+ points for central six crystals without veto cuts.

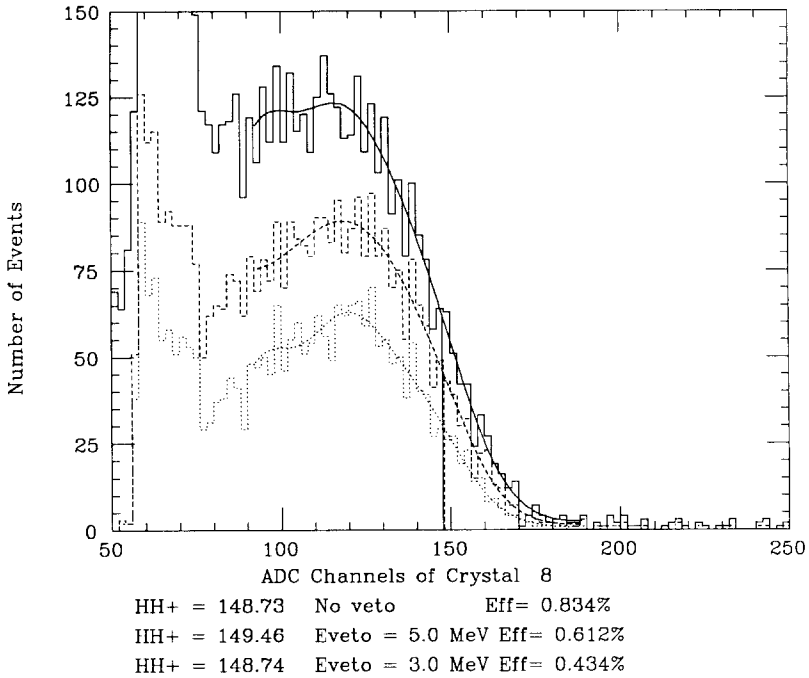

Fig. 13. A comparison of photon energy spectra of crystal 8 with different veto energy cuts.

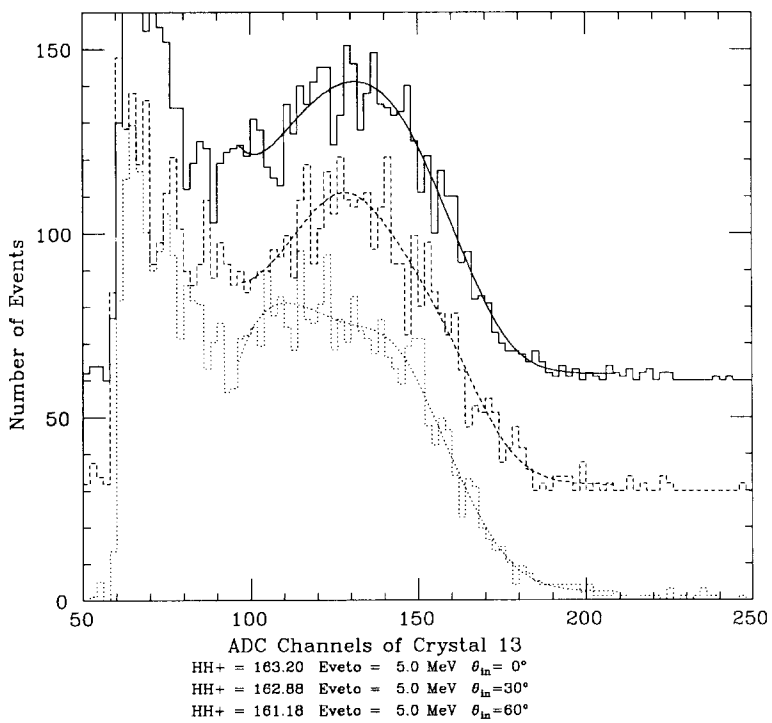

Fig. 14. A comparison of photon energy spectra of crystal 13 with 5 MeV veto cut for three different incident angles: 0° (solid line), 30° (dashed line) and 60° (dotted line). Note: the 0° and 30° spectra are shifted vertically by 60 and 30 counts respectively.

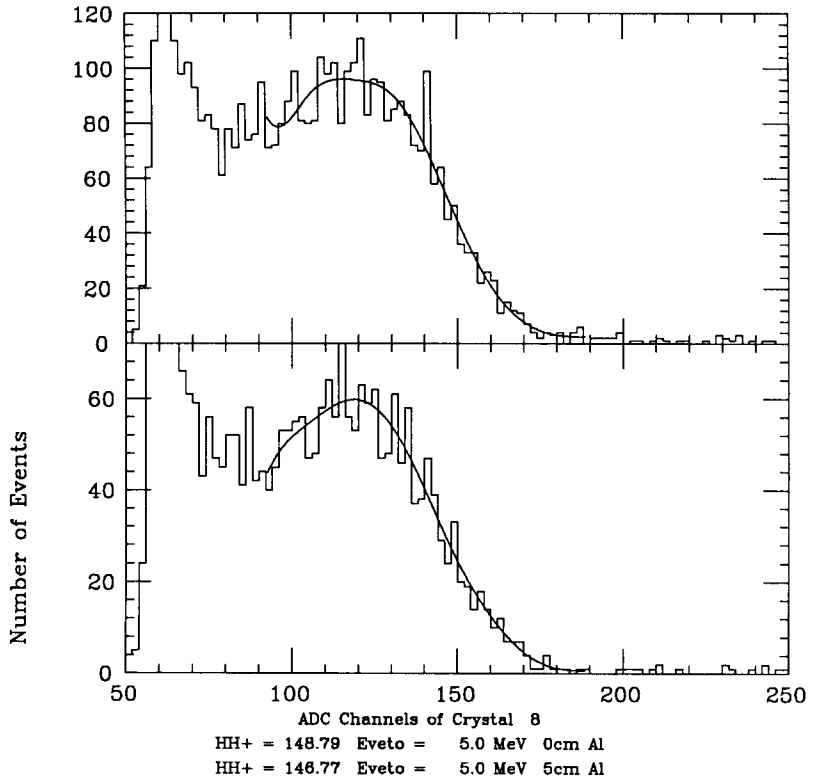

Fig. 15. A comparison of photon energy spectra of crystal 8 with 5 MeV veto cut for the cases with (bottom) and without (top) 5 cm aluminum in front.

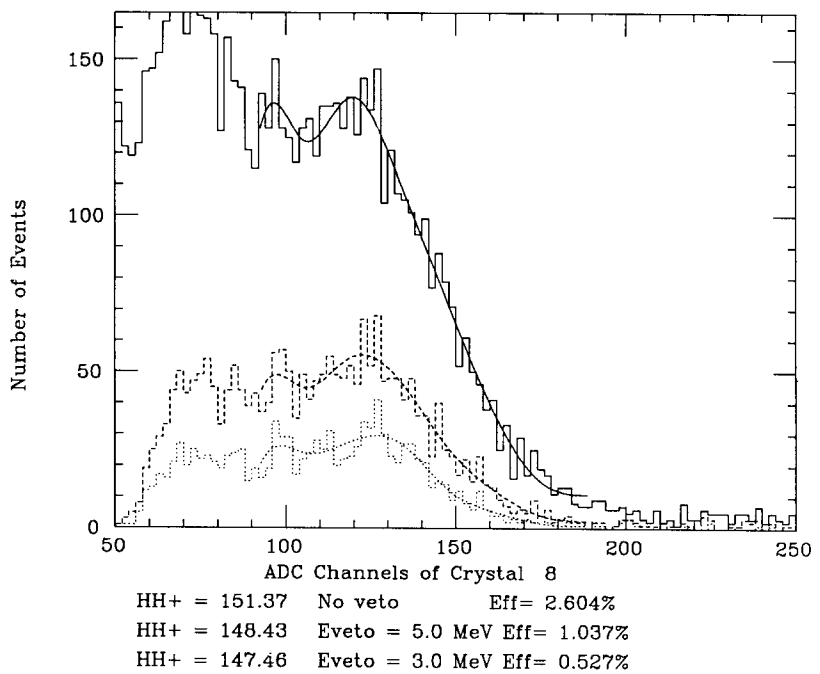

Fig. 16. The same as fig. 10, but with higher photon rate.

Table 5
The averaged HH^+ variation of the central six crystals in comparison with the Monte Carlo simulation [6]

Case	3 MeV veto		5 MeV veto		No. veto	
	M.C.	Data	M.C.	Data	M.C.	Data
30°	−0.7	−0.6	−0.8	−0.6	−0.9	−1.3
50°	−1.8	−1.4	−2.2	−1.4	−2.4	−2.5
5 cm Al	−0.5	−1.2	−0.5	−1.1	−0.8	−1.6

Note: The statistical error is about 0.8%.

Fig. 14 shows a comparison of three spectra obtained from crystal 13 for three different incident angles: normal, 30° and 60° respectively. The reason for choosing crystal 13 instead of crystal 8 is that crystal 13 was better shielded by two rows of crystals when the matrix was tilted by 60° with respect to the beam. The decrease of the HH^+ point with increasing incident angle is as predicted by the Monte Carlo simulations.

Fig. 15 illustrates the effect of having 5 cm aluminum in front of the crystal matrix. The decrease of the HH^+ points caused by the aluminum agrees with the Monte Carlo predictions.

Fig. 16 shows a comparison of spectra for a high photon rate run under veto cut conditions similar to fig. 13. The large hit probability, 2.6% per pulse before veto, and the visible tail at the upper end of the spectrum indicate that there was a significant contribution from double hits. Although the HH^+ point obtained from the spectrum without veto is shifted to a slightly higher value, it recovers when a 3 or 5 MeV veto cut is applied. The resultant efficiency and the HH^+ points are very close to the values obtained with normal beam intensity. Since the distance from the crystals and the target varies in the L3 detector, the photon rate cannot be optimized for all the crystals. The Veto cut is thus necessary to get stable calibration points for all the crystals.

Table 5 shows the close agreement between the small variations of the experimental HH^+ values obtained from an average of six central crystals under several running conditions and the variations predicted by the Monte Carlo simulations.

5.4. Systematic error of the calibration

As discussed in section 3, the effect of the incident photon angle and the presence of aluminum are fixed for each crystal in the experiment, so they will not result in a systematic calibration error. Overall, the systematics will be dominated by the long term stability. Within the limited time (several days) as AccSys the stability of the system appeared to be excellent.

Table 6 lists the HH^+ points of the central 6 crystals in the array, without veto cut, for different run conditions. Also listed in the table are the statistical deviations extracted from two identical runs. The absolute average of all 24 deviations in the table is 0.8%. 1% stability has therefore been achieved. Table 7 shows the corresponding data after the application of a 5 MeV veto cut. The absolute average deviation of 0.7% is limited by the statistical errors in the runs.

5.5. Future developments

A final test of the RFQ calibration technique, with 49 production-quality L3 crystals, is in preparation at Caltech. A new readout system, capable of reading out 49 crystals at a rate of more than 150 Hz has been developed and the new array of crystals is completed. The test run at AccSys, Inc. is scheduled for August 1988. Sufficient statistics will be acquired in order to test the calibration accuracy to 0.5%.

Table 6
HH^+ points of the central six crystals with no veto cut for normal incident, 30° and 50° incident photons and 5 cm Al in front of the matrix

Run	Comment	Crystal Number					
		7	8	9	12	13	14
2	Normal	143.4	147.8	135.0	137.0	162.0	126.3
7		145.4	149.7	135.0	139.8	163.1	128.2
	Deviation [%]	0.9	0.9	0.0	1.4	0.5	1.1
4	30°	145.2	148.3	135.5	135.1	161.9	126.1
9		144.6	148.2	136.9	136.1	161.4	125.5
	Deviation [%]	0.3	0.0	0.7	0.5	0.2	0.3
3	50°	142.8	148.6	131.8	133.7	156.9	123.8
10		147.4	148.4	135.0	135.2	159.6	125.8
	Deviation [%]	2.3	0.1	1.7	0.8	1.2	1.1
5	5 cm Al	142.9	146.7	128.0	136.9	160.7	127.2
13		143.9	145.2	130.4	135.6	162.4	125.7
	Deviation [%]	0.5	0.7	1.3	0.6	0.7	0.8

Note: The average deviation is 0.8%.

Table 7
HH^+ points of the central six crystals with 5 MeV veto cut for normal incident, 30° and 50° incident photons and 5 cm Al in front of the matrix

Run	Comment	Crystal number					
		7	8	9	12	13	14
2	Normal	142.8	148.8	134.4	137.2	162.4	127.0
7		145.7	150.2	137.4	139.7	163.2	127.9
	Deviation (%)	1.4	0.7	1.6	1.3	0.4	0.5
4	30°	144.6	147.9	136.2	138.1	164.3	125.8
9		144.9	148.2	136.8	135.6	162.9	126.7
	Deviation (%)	0.2	0.1	0.3	1.3	0.6	0.5
3	50°	143.8	149.0	132.3	135.5	157.3	125.8
10		145.1	149.4	134.1	139.1	160.0	127.4
	Deviation (%)	0.7	0.2	1.0	1.9	1.1	0.9
5	5 cm Al	143.9	146.8	132.9	136.9	160.6	127.3
13		143.0	146.0	132.1	137.5	163.7	126.9
	Deviation (%)	0.5	0.2	0.4	0.3	1.4	0.5

Note: The average deviation is 0.7%.

A complementary mode of operation of the system, in which a much greater flux of 6 MeV photons from a fluoride target may be used to simulate a 3–10 GeV single photon (through piling up of many photons in a gate) will also be tested. This mode of operation may be important for future use in the calibration of BaF_2 calorimeters at the SSC or LHC.

Acknowledgements

We are grateful to the L3 BGO group, especially collaborators from the Aachen, Annecy, Lyon and Princeton groups, for providing us with the necessary hardware components for the construction of the test matrix and readout system. We would like to thank Profs. C. Barnes and R. Kavanagh for many useful discussions and for providing us with the Van de Graaff facility at Kellogg Lab at Caltech. Dr. R. Sumner gave us many useful suggestions and helped us to build the readout system. The assistance of S. Sondergaard and many other technical staff members at Caltech and AccSys is greatly appreciated.

Last, but not the least, we would like to thank Prof. S.C.C. Ting for his continuous encouragement and support throughout all phases of this project.

Appendix A. Spline fit and statistical error

A cubic spline fit is applied to the upper edge of the spectrum, which usually included about 100 ADC channels, giving 50 bins if two bins are combined.

A spline function of degree k with n nodes has the properties:

- $S(x)$ is defined in the interval $\langle x_j, x_{j+1}\rangle$, $j = 1, \cdots, n-1$, as a polynomial of degree k;
- $S(x)$ has continuous derivatives of order up to $k-1$.

For a cubic spline with n nodes, there are $n-1$ different polynomials. The number of parameters that completely describe the function is reduced from $4(n-1)$ to $n+2$ by using the continuity of the function and its derivatives up to the second order. For our applications two end point conditions are given, reducing the number of parameters to be determined to n.

As a crosscheck, B-spline functions are also used to fit the spectrum. A cubic B-spline function is defined as

$$b_j(x) = \begin{cases} \frac{1}{6}z^3 & z=(x-x_j)/d, \\ & x_j < x < x_{j+1}, \\ \frac{1}{6}\{1+3[1+z(1-z)]z\} & \\ & z=(x-x_{j+1})/d, \\ & x_{j+1} < x < x_{j+2}, \\ \frac{1}{6}\{1+3[1+z(1-z)](1-z)\} & \\ & z=(x-x_{j+2})/d, \\ & x_{j+2} < x < x_{j+3}, \\ \frac{1}{6}(1-z)^3 & z=(x-x_{j+3})/d, \\ & x_{j+3} < x < x_{j+4}, \\ 0 & \text{otherwise}, \end{cases} \tag{1}$$

where x_j are the nodes with equal displacement d.

A function can be approximated by the superposition of a set of B-spline functions,

$$S(x) = \sum_{j=1}^{n} p_j b_j(x), \tag{2}$$

where p_j are the parameters, j goes over all the nonzero $b_j(x)$ functions for a given x, and $n = N_{\text{int}} + 3$ with N_{int} being the number of intervals in the region.

In both cases, the function can be written as,

$$y = S(x, \boldsymbol{p}) \tag{3}$$

where $\boldsymbol{p} = \{p_i\}$ is a set of parameters.

To determine the parameters p_i, x^2 is minimized.

$$\chi^2 = \sum_{i=1}^{N_b} \frac{[S(x_i, \boldsymbol{p}) - y_i]^2}{\delta y_i^2}, \tag{4}$$

$$\frac{\partial \chi^2}{\partial p_j} = \sum_{i=1}^{N_b} \frac{2[S(x_i, \boldsymbol{p}) - y_i]}{\delta y_i^2} \frac{\partial S(x_i, \boldsymbol{p})}{\partial p_j}, \quad = 0 \tag{5}$$

where N_b is the total number of bins, y_i is the content in the ith bin in the energy spectrum, and δy_i is the associated error. For both fits, the above equations reduce to a set of linear equations. For simplicity, only the equations for the cubic B-spline fit are given below:

$$\mathbf{A}\boldsymbol{p} = \mathbf{B}, \tag{6}$$

where

$$A_{jk} = \sum_{i=1}^{N_b} \frac{b_j(x_i) b_k(x_i)}{\delta y_i^2}, \quad B_k = \sum_{i=1}^{N_b} \frac{y_i b_k(x_i)}{\delta y_i^2},$$

and

$$\boldsymbol{p} = \mathbf{A}^{-1}\mathbf{B}. \tag{7}$$

The statistical errors of the parameters $\boldsymbol{p}$ are correlated in general. The error matrix σ_{ij} is written as the inverse matrix of the second derivatives of χ^2:

$$\{\sigma_{ij}\} = \left\{ \frac{1}{2} \frac{\partial^2 \chi^2}{\partial p_i \partial p_j} \right\}^{-1}. \tag{8}$$

The peak of the spline (y_{max}, x_{max}) satisfies

$$\frac{\partial S}{\partial x_{max}} = 0, \tag{9}$$

$$y_{max} = S(x_{max}, \boldsymbol{p}). \tag{10}$$

With x_{max} given by the above equation, the HH^+ point is then the root of the following equation:

$$\tfrac{1}{2} S(x_{max}, \boldsymbol{p}) = S(x_{HH^+}, \boldsymbol{p}). \tag{11}$$

The error of x_{HH^+} depends on the parameters and their error matrix.

$$\frac{\partial x_{HH^+}}{\partial p_i} = \left\{ \frac{1}{2} \left[\frac{\partial S(x_{max}, \boldsymbol{p})}{\partial x_{max}} \frac{\partial x_{max}}{\partial p_i} + \frac{\partial S(x_{max}, \boldsymbol{p})}{\partial p_i} \right] - \frac{\partial S(x_{HH^+}, \boldsymbol{p})}{\partial p_i} \right\} \left\{ \frac{\partial S(x_{HH^+})}{\partial x_{HH^+}} \right\}^{-1}. \tag{12}$$

$$\Delta x_{HH^+} = \sqrt{\sum_{i,j=1}^{n} \frac{\partial x_{HH^+}}{\partial p_i} \frac{\partial x_{HH^+}}{\partial p_j} \sigma_{ij}}. \tag{13}$$

The results of the calculation are shown in table 4, where the statistical errors obtained from different methods are compared for the central six crystals in run 7. It is clear from the table that the statistical error of the HH^+ point is about 0.8%.

References

[1] L3 Collaboration, L3 Technical Proposal, May 1983;
J. Bakken et al., Nucl. Instr. and Meth. A254 (1987) 535 and 228 (19850 294.

[2] G.J. Bobbink et al., Nucl. Instr. and Meth. 227 (1984) 470.

[3] C. Laviron and P. Lecoq, Nucl. Instr. and Meth. 227 (1984) 45;
Kobayashi et al., Nucl. Instr. and Meth. 206 (1983) 107;
C. Bieler et al., Nucl.Instr. and Meth. A234 (1985) 435.

[4] T.Q. Zhou et al., LEP3 Internal Report, November 1984, and Nucl. Instr. and Meth. A258 (1987) 58.

[5] The BGO crystals for the L3 electromagnetic calorimeter have been produced at the Shanghai Institute of Ceramics (SIC) in China. Recent developments at SIC indicate that the L3 BGO crystals in the end caps of the calorimeter, which are now being produced, will have improved radiation resistance.

[6] R.Y. Zhu, EGS Study on the BGO Calibration by Using Low Energy Photons, L3 internal report, December 1985.

[7] AccSys Technology, Inc., 1177 Quarry Lane, Pleasanton, CA 94566, USA.

[8] Los Alamos National Laboratory, Collection of papers on the RFQ Linear Accelerator, Presented by Accelerator Technology Division Personnel, March 1979–May 1983.

[9] Electron gamma shower (EGS) program, by R. Ford and W. Nelson. See Report SLAC-210, EGS Code System (version 3), June 1978.

[10] H. Newman and R.Y. Zhu, Proposal for a BGO Calibration Test at AccSys, October 1987.

[11] L3/Princeton Group, Noise Studies - Autumn 1987, L3 internal report, February 1988.

[12] A well-shielded rf system will reduce the rf pickup by a factor of 80 dB.
J. Potter, private communication.